Journal of Structural Geology 32 (2010) 693–702

Contents lists available at ScienceDirect

Journal of Structural Geology

journal homepage: www.elsevier.com/locate/jsg

Palaeostress perturbations near the El Castillo de las Guardas fault (SW Iberian Massif)

Encarnación García-Navarro*, Carlos Fernández

Departamento de Geodinámica y Paleontología, Universidad de Huelva, 21071-Huelva, Spain

ARTICLE INFO

Article history:
Received 23 June 2009
Received in revised form
7 April 2010
Accepted 11 April 2010
Available online 18 April 2010

Keywords:
Fault
Palaeostress
Stress trajectories
Iberian Massif

ABSTRACT

Use of stress inversion methods on faults measured at 33 sites located at the northwestern part of the South Portuguese Zone (Variscan Iberian Massif), and analysis of the basic dyke attitude at this same region, has revealed a prominent perturbation of the stress trajectories around some large, crustal-scale faults, like the El Castillo de las Guardas fault. The results are compared with the predictions of theoretical models of palaeostress deviations near master faults. According to this comparison, the El Castillo de las Guardas fault, an old structure that probably reversed several times its slip sense, can be considered as a sinistral strike-slip fault during the Moscovian. These results also point out the main shortcomings that still hinder a rigorous quantitative use of the theoretical models of stress perturbations around major faults: the spatial variation in the parameters governing the brittle behaviour of the continental crust, and the possibility of oblique slip along outcrop-scale faults in regions subjected to general, non-plane strain.

1. Introduction

Brittle fracture of crustal rocks is a process controlled by physical parameters and relations (confining pressure, pore pressure, strain rate, temperature, differential stress, stress changes, friction and elastic coefficients, among many others) whose exact values are largely unknown for a given rock massif, and only general friction laws are available (Byerlee, 1978; Scholz, 1990; Engelder, 1993). These parameters condition the attitude of fractures, their displacement, and the triggering of seismic events (Pollard and Segall, 1987; Cowie and Scholz, 1992; King et al., 1994). Rock massifs are geometrically and mechanically heterogeneous (e.g., Bieniawski, 1989) and, hence, deviation of stress fields are common in fractured areas (Zoback et al., 1987; Homberg et al., 1994). Major faults are commonly composed of distinct segments that can show independent slip (Schwartz and Sibson, 1989).

Apart from these complexities, the conditions under which failure occurs in rocks are characterised by the widely used Coulomb failure criterion. Rocks deformed experimentally are shown to approximately obey this criterion (e.g., Jaeger and Cook, 1979). The stress deviation near the tip of pre-existing faults can be theoretically modelled in an elastic half space containing a fault that accomplishes the Coulomb criterion and is subjected to slip under an external stress field. As a consequence of this line of research, it has been observed that a cortege of secondary fractures and other geological structures can appear near the tips of the slipped segment (Anderson, 1951; McKinstry, 1953; Chinnery, 1966; Price, 1968; Lajtai, 1968). More recent models analyse the influence of the distinct physical parameters and the geometry of the stress trajectories around faults (e.g., Pollard and Segall, 1987; Mandl, 1988; Petit and Barquins, 1990; Homberg et al., 1997, 2004; Toda and Stein, 2002; Maerten et al., 2002). Study of second order structures (stylolites, tension gashes, dykes, joints, minor faults) at relevant field cases has allowed determining stress-field deviations near natural faults (e.g., Petit and Mattauer, 1995; Casas-Sáinz and Maestro-González, 1996; Simón et al., 1999). Knowledge of the geometry of stress perturbations obtained from the study of second order structures can be used to deduce the slip sense of old, major faults.

This work describes the stress field associated with the displacement of a major fault during Late Variscan times, the El Castillo de las Guardas fault. Second order faults are analysed using techniques of fault-slip inversion. Several dyke systems were emplaced coeval to these faults. Dyke and fault data are used to determine stress trajectories and the results are tested against the predictions of the theoretical models of Homberg et al. (1997) and Toda and Stein (2002).

* Corresponding author.
E-mail address: navarro@uhu.es (E. García-Navarro).

0191-8141/$ – see front matter © 2010 Elsevier Ltd. All rights reserved.
doi:10.1016/j.jsg.2010.04.004

2. Geological setting

2.1. General features

The South Portuguese Zone is located at the southernmost part of the Variscan Iberian Massif (Julivert et al., 1974). The northern boundary of the South Portuguese Zone (Fig. 1) has been interpreted as a Variscan tectonic suture (Bard, 1969; Crespo-Blanc and Orozco, 1991; Díaz-Azpiroz et al., 2006; Ribeiro et al., 2007). The South Portuguese Zone is considered as a part of a Variscan orogenic wedge (Simancas et al., 2003) subjected to an intense progressive deformation that evolved from large-scale lateral convergence of continental blocks to an essentially transcurrent tectonics late during the Variscan orogenesis (García-Navarro and Fernández, 2004; Mantero et al., 2007). The rocks of the South Portuguese Zone are Devonian and Carboniferous and include sedimentary and igneous protholiths variably affected by the Variscan deformation and metamorphism. Structurally, the South Portuguese Zone is a fold and thrust belt, vergent to the south and southwest, and generated in response to thin-skinned tectonics (Silva et al., 1990; Quesada, 1998; Simancas et al., 2003). The Castilblanco de los Arroyos batholith (de la Rosa, 1992), composed of a large variety of basic to acid igneous rocks, intruded at shallow crustal levels the rocks of the South Portuguese Zone (Fig. 1). Intrusion ages range from Late Visean to Moscovian (de la Rosa, 1992; Giese et al., 1993), although most of the batholith was emplaced during the Bashkirian and Moscovian, and its external contacts crosscut the Variscan folds and thrusts. The rocks of the Castilblanco de los Arroyos batholith were affected by a brittle deformation that has been considered as the last stage of the Variscan orogeny (García-Navarro and Fernández, 2004). This brittle deformation stage lasted from the Moscovian to the Permian and it consisted of several phases of transtension and transpression, accompanied by the intrusion of distinct systems of basic dykes (García-Navarro et al., 2003). Finally, the eastern part of the South Portuguese Zone was covered by the post-orogenic Early Permian sediments of the Viar basin, which mostly postdate the aforementioned brittle deformation phases. The Neogene sediments of the Guadalquivir basin unconformably cover the southern boundary of the South Portuguese Zone (Fig. 1).

2.2. Faults and diabase dykes at the eastern part of the South Portuguese Zone

The major fractures outcropping at the eastern part of the South Portuguese Zone are (Fig. 1): the Southern Iberian shear zone, the El Garrobo-Burguillos shear zone, the Cala dam fault, and the El Castillo de las Guardas fault. The Southern Iberian shear zone marks the northern limit of the South Portuguese Zone and it was generated during the main stages of the Variscan collision (Crespo-Blanc and Orozco, 1988; Díaz-Azpiroz and Fernández, 2005). The El Garrobo-Burguillos shear zone is N110°E-striking, and it is characterised by a plano-linear ductile fabric with associated kinematic criteria indicating a predominant strike-slip, sinistral displacement. Later brittle overprinting of the ductile structures shows dextral slip. The Cala dam fault is a sinistral strike-slip fault, with a minimum length of 20 km. The azimuth of this fault varies from N40°–50°E (southwest) to N60°–65°E (northeast). The analysis of the geological map (Fig. 1) allows estimating a horizontal displacement of around 7 km for the Cala dam fault. Most of this displacement took place early during the Late Variscan brittle deformation, because the Cala dam fault was unfavourably oriented for slip after the Moscovian (García-Navarro and Fernández, 2004). The Early Permian sediments of the Viar basin cover the northeastern tip of the Cala dam fault. The El Castillo de las Guardas fault, a largely strike-slip structure, shows a minimum length of 46 km and its average azimuth is N130°E, parallel to the southern boundary of the Castilblanco de los Arroyos batholith. Notwithstanding, some segments of the El Castillo de las Guardas fault are E-W-oriented, and its southern tip is covered by the Neogene sediments of the Guadalquivir basin. It is not possible to determine the magnitude of displacement along the El Castillo de las Guardas fault due to the absence of suitable markers. Furthermore, displacement along the El Castillo de las Guardas fault has alternated between sinistral and dextral during the Late Carboniferous and Early Permian (García-Navarro and Fernández, 2004), which complicates the determination of the amount of slip for each episode.

The Southern Iberian shear zone was disrupted by an en échelon system of brittle, sinistral, NE-SW directed faults (Simancas, 1985).

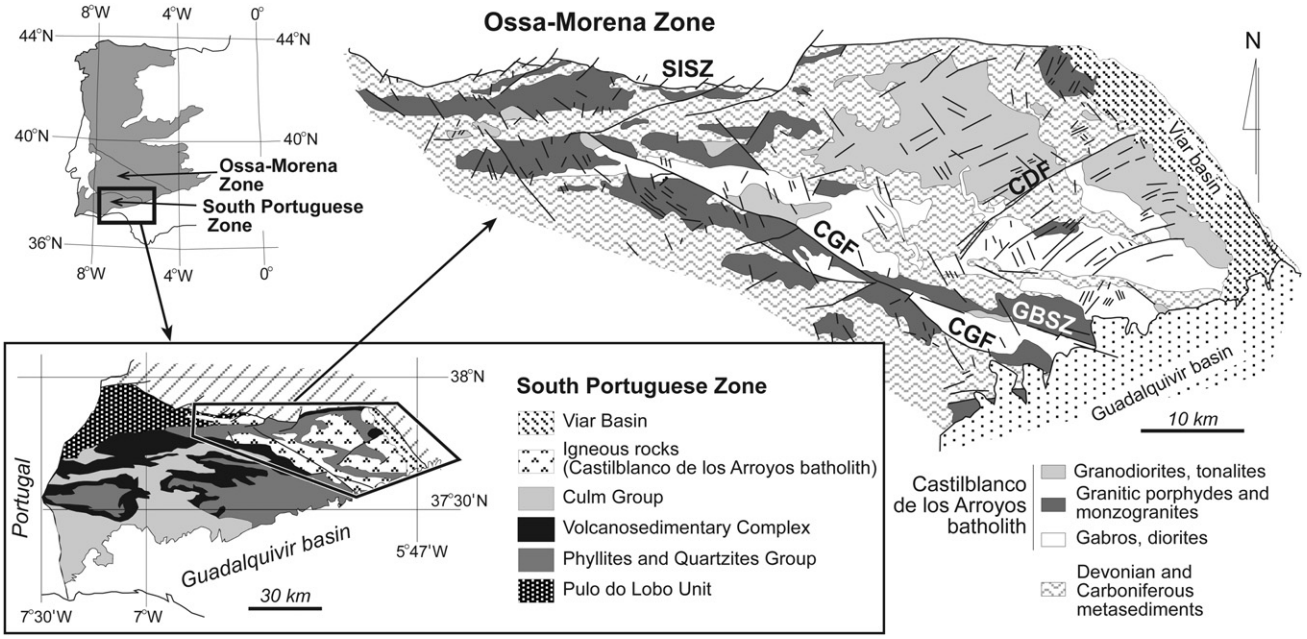

Fig. 1. Geological map of the northeastern part of the South Portuguese Zone, with location of the major faults and ductile shear zones (Southern Iberian shear zone, SISZ; El Castillo de las Guardas fault, CGF; El Garrobo-Burguillos shear zone, GBSZ; and the Cala dam fault, CDF).

The western tip of the El Garrobo-Burguillos shear zone is crosscut by the El Castillo de las Guardas fault. Therefore, it can be concluded that both ductile shear zones are older than the brittle structures generated during the Moscovian-Permian deformation stage. Splay faults can be observed at the southwestern termination of the Cala dam fault (Fig. 1), which ends in the middle of the Castilblanco de los Arroyos batholith. Therefore, time relationships between the Cala dam and the El Castillo de las Guardas faults cannot been constrained from field evidence, although indirect information can be obtained from the analysis of outcrop-scale faults and dykes, as indicated below in this section.

The relative age of the distinct basic (diabase) dyke systems intruding the Castilblanco de los Arroyos batholith can be obtained from crosscutting relationships among them. The strike of the older dyke system is NE-SW to ENE-WSW, while the NNE-SSW to N-S directed dykes are more recent. The younger dyke system is NW-SE oriented. In all cases, the dykes are sub-vertical.

Outcrop-scale faults are arranged in several systems. García-Navarro and Fernández (2004) distinguished three main fault systems, called A, B and C. Relative age between these three fault systems can be obtained by studying the mutual crosscut relationships among faults and faults and dykes (García-Navarro and Fernández, 2004). Absolute dating of the rocks of the Castilblanco de los Arroyos batholith, the syntectonic sediments of the South Portuguese Zone and the materials of the Viar basin (Simancas, 1983; Colmenero et al., 2002; Sierra, 2003), allowed García-Navarro and Fernández (2004) to sharply constrain the age of each fault system, which be assumed in this work. Fault system A is the older one (Moscovian), and it is contemporary with the NE-SW to ENE-WSW-striking diabase dykes. Fractures of system A are essentially strike-slip faults. Most of them are sinistral, ESE-WNW to ENE-WSW-directed faults, although dextral, N-S-oriented faults are also present. Sinistral, NW-SE-directed faults can be observed in the vicinity of some major faults. Dykes and faults of system A show contrasted azimuths and are kinematically compatible. Locally, some faults with a dominant normal dip-slip component of displacement can trend sub-parallel to adjacent contemporary dykes. The first stage of activity of the El Castillo de las Guardas fault and the main displacement along the Cala dam fault were coeval to this Moscovian system of small-scale faults. Faults of system B are younger (Kasimovian to Gzhelian) than those of system A. System B is formed by dextral, NW-SE-striking faults. Finally, the NW-SE and N-S-directed faults of system C are the youngest (Gzhelian to Early Permian), and affected the older materials of the Early Permian Viar basin. As explained before, the El Castillo de las Guardas fault experienced reactivations contemporary with those systems B and C of small-scale faults.

The aim of this work is to use the faults of system A to obtain a map of the stress trajectories at the eastern part of the South Portuguese Zone during the Moscovian. Only the faults belonging to this system A have been considered at each outcrop to determine the stress field. In particular, the perturbation of these stress trajectories near the El Castillo de las Guardas fault during the first stage of its activity will be discussed and interpreted.

3. Methodology and results

Outcrop-scale faults of system A have been measured at 33 sites (Fig. 2). The younger faults (systems B and C) measured at the distinct sites have been thrown out of ensuing calculations. Measurement at each site includes fault azimuth and dip as well as slip orientation and sense (Fig. 3). One method of fault slip data inversion has been applied. The stress inversion method of Reches et al. (1992) consists in determining the stress tensor knowing the direction and sense of slip on a fault population. The faults are then represented on the Mohr diagram to check their mechanical compatibility with the determined stress tensor. Faults of system A are the older outcrop-scale structures in the studied area, affecting slightly older plutonic rocks. Therefore, they are likely neoformed faults. Neoformed fault sets commonly show orthorhombic (four sets, general deformation) or monoclinic (two sets, plane deformation) symmetries (Hancock, 1985; de Vicente, 1988; Krantz, 1988; Marrett and Allmendinger, 1990; Angelier, 1994; Nieto-Samaniego, 1999). Similar patterns have been obtained in triaxial experiments in intact rock (Reches and Dieterich, 1983). However, it is not always possible to observe the four fault sets with orthorhombic symmetry in the field, mainly due to the cut effect and other deficiencies of exposures (Camacho, 1999). In that case, the fault slip data inversion methods can yield inclined principal stress axes (Twiss and Unruh, 1998; Camacho, 1999). To avoid spurious variations in the location of the principal stress axes determined from the method of Reches et al. (1992) due to measurement of incomplete fault systems, the corrections suggested by Camacho (1999) have been applied. Apart form this, the basic dykes can be considered as type I fractures (Pollard and Segall, 1987). Accordingly, the pole to the dyke boundary coincides with the least compressive stress axis (σ_3).

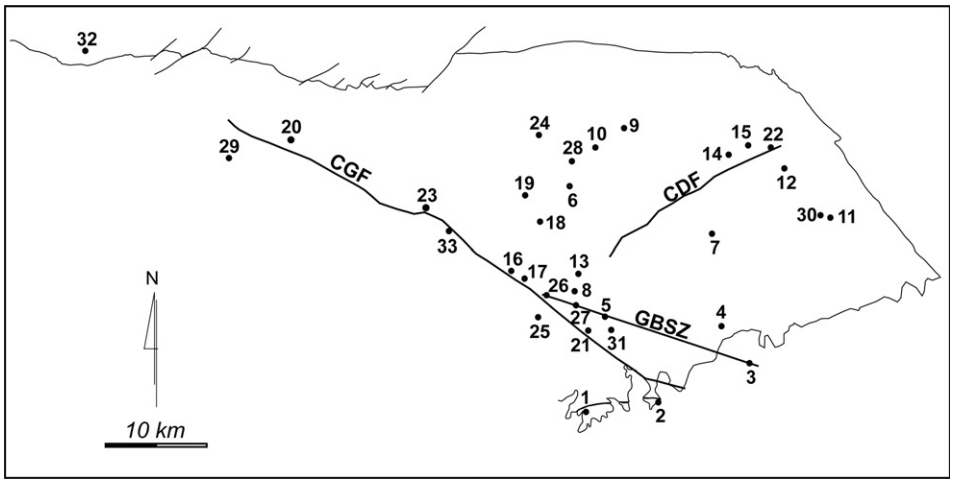

Fig. 2. Sketch based on the map of Fig. 1 showing the location of the 33 fault measurement sites at the studied area.

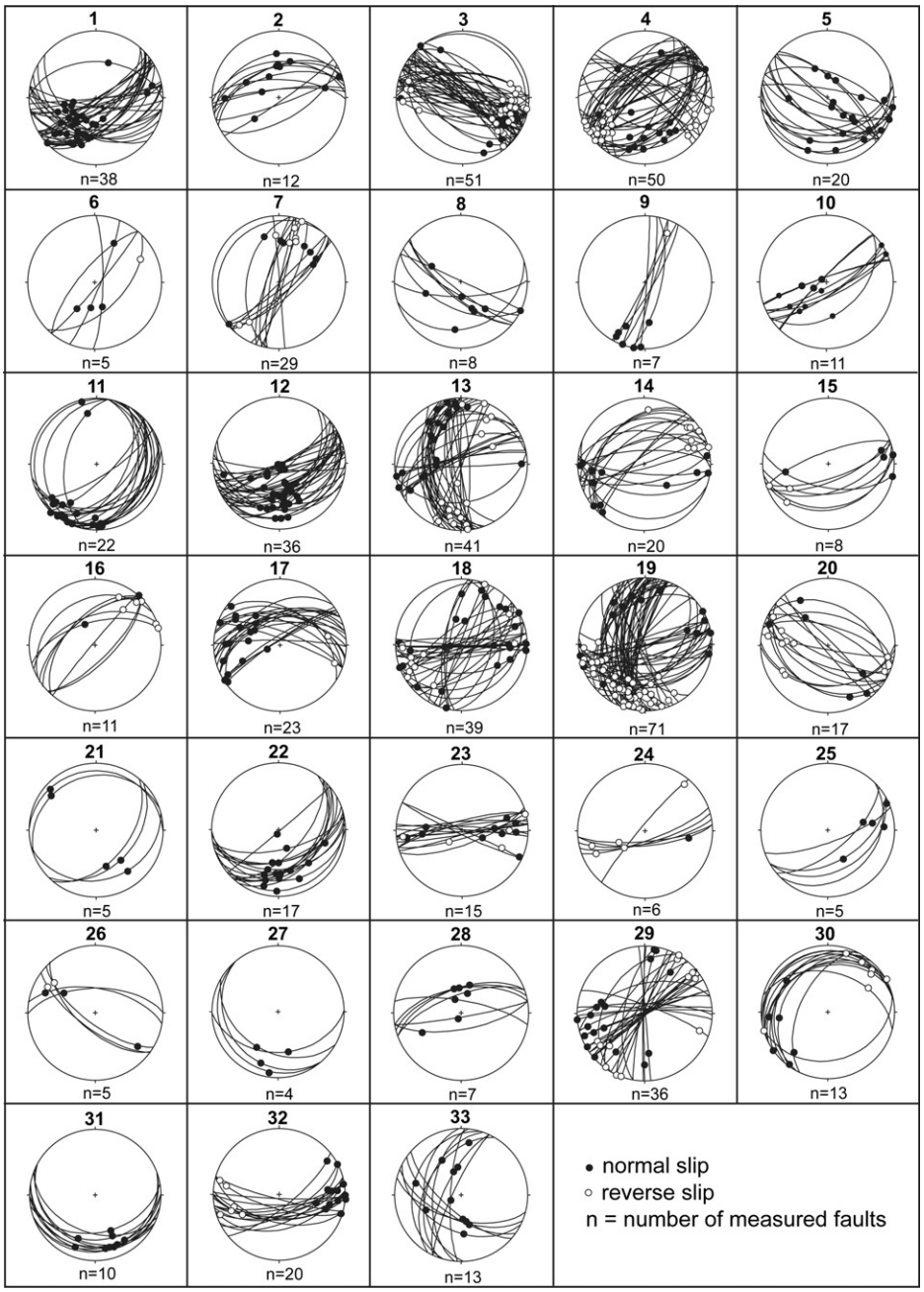

Fig. 3. Equal area, lower hemisphere plots with the cyclographic projection of the faults measured at each site (see location in Fig. 2), with indication of the slickenside striations and slip sense.

Most faults measured in this work are oblique-slip faults with a normal dip-slip component (Fig. 3). Strike-slip reverse and pure normal faults have also been observed. The attitude of the stress axes determined with the previously described fault slip data inversion methods agree with this general description (Table 1). Accordingly, the maximum horizontal stress axis (S_H) coincides with either the maximum (σ_1) or the intermediate (σ_2) principal stress axes. The software proposed by Lee and Angelier (1994) has been used to reconstruct trajectories of S_H at the studied area (Fig. 4). Fault and dyke analysis yield similar patterns of stress trajectories (compare Fig. 4A, B and Fig. 4C). The average regional S_H azimuth is N55°E, although some stress perturbations can be observed around the El Castillo de las Guardas fault, in particular at its tips and near its central curved segment. The distribution of fault measurement sites is highly unequal due to exposure reasons. Accordingly, only a few appropriate sites have been found at the northwestern tip of the El Castillo de las Guardas fault. This limitation is partially overcome by the quality of these measurement sites (20 and 29, Fig. 3), with a set of internally consistent faults, easy to interpret with the used stress inversion methods. Also diabase dykes yield a similar pattern of stress trajectories at the northwestern termination of the El Castillo de las Guardas fault (Fig. 4C). Besides, sites with a small number of measured faults (<10) are located far from fault tips, where stress perturbations are less important and a larger coverage of measurement sites is available. Therefore, the stress trajectory maps shown in Fig. 4 are

Table 1
Results of the application of the method of Reches et al. (1992) and of Camacho (1999) to the faults measured at the distinct sites located in Fig. 2. The results of the best fit between the measured faults and the predictions of the "Coulomb 2.5" program (Toda and Stein, 2002) are also shown.

Measurement sites	n	Stress inversion method (Reches et al., 1992)					Coulomb 2.5 Program	Camacho (1999)
		σ_1	σ_2	σ_3	R	μ	S_H	S_H
1	38	68/288	21/099	03/190	0.36	0.3	47(σ_2)	99±1(σ_2)
2	12	66/065	22/230	05/322	0.29	0.8	52(σ_2)	42.5± 2.5(σ_2)
3	51	13/069	65/308	20/164	0.24	0.1	44(σ_2)	80± 4(σ_1)
4	50	39/277	45/065	16/173	0.86	0.2	47(σ_2)	82(σ_1)
5	20	56/107	28/254	15/352	0.11	0.8	20(σ_2)	83(σ_2)
6	5	76/248	13/064	00/154	–	–	56(σ_1)	–
7	29	85/049	04/223	00/313	0.15	0.9	55(σ_2)	37.5± 2.5(σ_2)
8	8	80/191	00/286	09/016	0.26	0.7	45(σ_2)	92± 1(σ_2)
9	7	69/198	20/035	05/303	0.67	1.7	53(σ_1)	20(σ_2)
10	11	75/198	12/051	07/319	0.4	1.2	53(σ_1)	46(σ_2)
11	22	40/201	17/095	44/348	0.09	1.1	55(σ_1)	90± 0.5(σ_2)
12	36	80/236	09/071	02/341	0.21	0.5	58(σ_1)	79(σ_2)
13	41	14/221	73/006	09/129	0.66	0.2	47(σ_1)	41± 1(σ_1)
14	20	01/215	80/316	09/125	0.55	0.5	68(σ_1)	68±28(σ_1)
15	8	03/051	66/149	23/320	0.50	0.8	64(σ_2)	62±15(σ_1)
16	11	08/029	73/267	13/121	0.06	1.9	45(σ_1)	16±3(σ_1)
17	23	52/232	37/045	03/138	0.78	0.2	57(σ_1)	17±24(σ_2)
18	39	46/041	42/209	05/305	0.90	0.1	44(σ_1)	36(σ_2)
19	71	06/217	73/332	13/126	0.28	0.2	56(σ_1)	36±1(σ_1)
20	17	00/075	57/166	31/344	0.45	0.2	57(σ_2)	94±0.5(σ_1)
21	5	11/234	75/016	08/142	–	–	15(σ_2)	–
22	17	47/228	39/072	12/331	0.51	0.6	95(σ_2)	73±26(σ_2)
23	15	79/054	10/241	01/151	0.43	0.5	87(σ_1)	61(σ_2)
24	6	33/207	43/335	28/096	–	–	57(σ_1)	–
25	5	57/033	32/211	00/302	–	–	28(σ_2)	–
26	5	27/256	61/090	05/349	–	–	79(σ_1)	–
27	4	56/107	28/250	15/350	–	–	3(σ_2)	–
28	7	78/268	11/091	00/001	0.38	1.3	57(σ_1)	94(σ_2)
29	36	23/219	66/037	00/129	0.83	0.1	55(σ_2)	38(σ_1)
30	13	40/201	17/095	44/348	0.09	1.1	62(σ_1)	89(σ_2)
31	10	66/158	04/259	22/351	0.53	0.2	30(σ_2)	79(σ_2)
32	20	05/218	73/109	15/309	0.98	0.2	54(σ_1)	38(σ_1)
33	13	83/081	06/246	01/336	0.26	0.2	53(σ_1)	59(σ_2)

considered as fairly reliable. Similarly, the sinistral displacement of the Cala dam fault (N60°–65°E-trending) is mechanically compatible with the average azimuth of the average maximum horizontal stress (N55°E), although some stress perturbation (not detected in this work) should have been active at its southwestern tip, where the fault is branched and changes its strike. Interpretation of this stress perturbation as due to the presence of a large-scale discontinuity (the El Castillo de las Guardas fault) will be discussed in the next section.

4. Discussion

4.1. Theoretical models of stress perturbation around major faults

Earthquake triggering and complex fault interaction patterns have been described as a consequence of dynamic and static stress changes at fracture zones (Cocco et al., 1999). Scholz (1998) has shown the insensitivity of earthquakes to stress transients, while fault-slip triggering strongly depends on changes in static stress. Accordingly, several models have been presented that idealise fault displacement as a consequence of variations in the static stress necessary to produce slip along a given fault segment (Homberg et al., 1997, 2004; "Coulomb" software of Toda and Stein, 2002).

Homberg et al. (1997, 2004) reconstructed the local static stress field around a pre-existing vertical, strike-slip fault after sliding on it. The model considers plane deformation and satisfies the Mohr–Coulomb shear failure criterion with cohesion equalling zero along the discontinuity. The angle between the discontinuity and the regional S_H axis (θ) ranges between 0° and 90°. The applied regional differential stress (σ_1–σ_3) varies between 10 and 100 MPa, and the friction coefficient (μ) ranges from 0.01 to 1. Homberg et al. (1997, 2004) concluded that reactivation of pre-existing faults generates a characteristic perturbation of the static stress field around the fault, whose pattern is independent from θ, μ and the magnitude of the principal stress axes. Variation in these parameters can alter the degree of the stress field perturbation, but the basic pattern remains unchanged (Fig. 5). This pattern is defined by the following characteristics (Homberg et al., 2004): The deviation of stress trajectories is a maximum at the fault tips and it occurs near the discontinuity, affecting an area with a radius smaller than half the fault displacement. The stress distribution is symmetrical relative to the centre of the discontinuity. For a sinistral fault (Fig. 5) the S_H trajectory is rotated in a clockwise sense by an angle β in the contractional domain and anti-clockwise by and angle α in the extensional domain. The angles α and β can vary depending on θ, μ, and (σ_1–σ_3), although the location of the perturbations and the rotation sense are not affected. The amount of slip along the fault is believed to increase the extent of the stress perturbation and the value of angles α and β, however, the exact quantitative dependence of the stress perturbation on the distinct faulting parameters is largely unknown (Homberg et al., 1997). The model, nevertheless, can be used to identify old active faults or fault segments if the stress distribution around the discontinuity can be determined.

The model of Toda and Stein (2002) assumes that earthquake occurrence is related to changes in the Coulomb failure stress (ΔCFS) that can be defined as:

$$\Delta\mathrm{CFS} = \Delta\tau + \mu(\Delta\sigma_n + \Delta P) \quad (1)$$

where $\Delta\tau$ and $\Delta\sigma_n$ are the changes in the shear stress and normal stress on a fault, respectively. ΔP is the change in the pore fluid

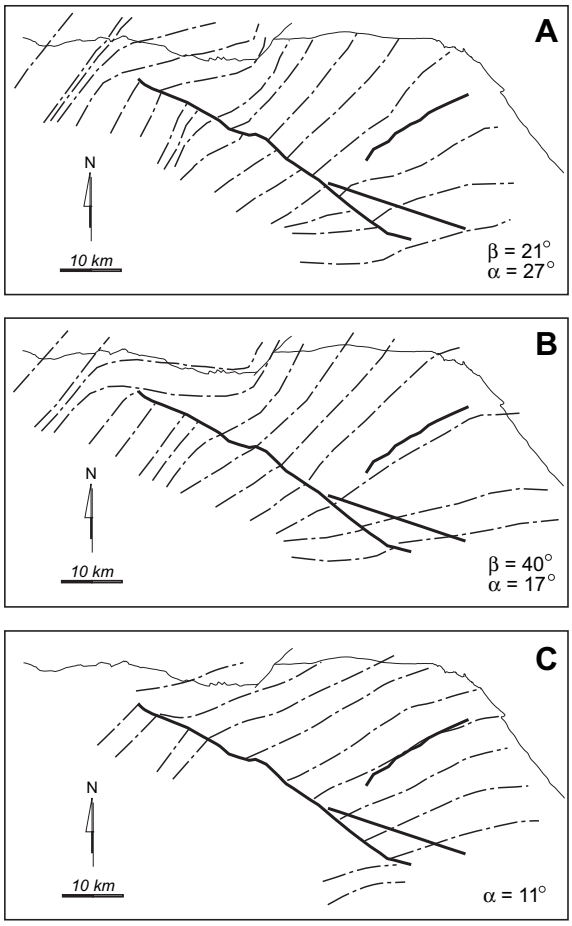

Fig. 4. Maps of S_H (maximum horizontal stress axis) trajectories interpolated using the method of Lee and Angelier (1994) from the results obtained at each measurement site. The techniques used to determine the stress at each site are: A) the method of Reches et al. (1992); B) the correction proposed by Camacho (1999) for incomplete fault systems; and C) the attitude of diabase dykes. Meaning of angles α and β is explained in Fig. 5 and in the text.

pressure. The model is implemented through the "Coulomb 2.5" software, which computes the deformation field and the static stress changes caused by slip along a major fault or along several coeval faults. It also allows determining the small-scale fault planes optimally oriented to slip after displacement along a master fault. ΔCFS values are a function of the fault geometry, slip sense and friction coefficient, but independent of the regional stress. Earthquake

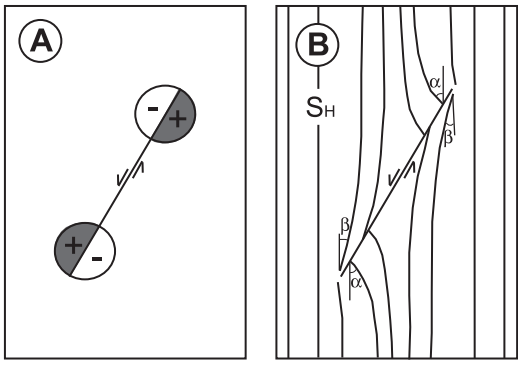

Fig. 5. Sketch depicting the results of the method of Homberg et al. (1997). A) Distribution of the extensional (−) and contractional (+) domains at the tips of a fault zone. B) stress field signature of a strike-slip fault (right). Angles α and β indicate the rotation of the regional σ_1 trajectories near the fault.

events promote a reduction of the shear stress on the fault plane and small changes of this stress component in nearby fault planes. Also the strike of the principal stress axes is rotated around the slipped fault segment. $\Delta\tau$ values are large enough to trigger or inhibit later events on optimally-oriented faults.

4.2. Evaluation of the stress fields at the studied area

The average regional S_H azimuth is N55°E at the studied zone, as stated above. The stress tensors determined with the use of the fault slip data inversion methods (Table 1) are in accordance with most of the measured faults that show a predominant strike-slip or normal component (Fig. 3). The attitude of the large-scale faults with respect to the S_H axis (the σ_1 or the σ_2 axes), and their projection on the Mohr space (Fig. 6) suggests that they are reactivated faults. The El Castillo de las Guardas faults and the El Garrobo-Burguillos shear zone define the southern limit of the Castilblanco de los Arroyos batholith (Fig. 1). The Cala dam fault separates two domains of the batholith, with he basic rock facies (gabbros and diorites) almost absent to the northwest of this fault (Fig. 1). Indeed, the master faults analysed in this work are old structures deeply entrenched in the crust (Ábalos and Díaz Cusí, 1995). They are prone to slip under distinct stress fields. After the intrusion of the Castilblanco de los Arroyos batholith, the first stage of brittle deformation generated displacement along these large old faults. The resulting deviation in the stress trajectories originated the neoformed, small-scale faults of system A measured in this work. The aim of this section is to compare the stress trajectories

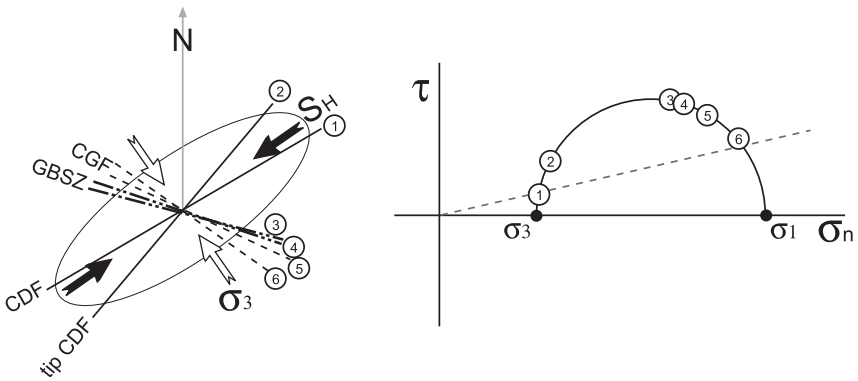

Fig. 6. A) Azimuth of the major faults (acronyms as in Fig. 1) relative to the average attitude of the maximum horizontal stress axis ($S_H \approx \sigma_1$ or σ_2). B) Projection in the Mohr space (not to scale) of the major faults with respect to the average stress ($\mu = 0.5$).

determined here from the study of the small faults of system A with the theoretical stress pattern predicted by the models of Homberg et al. (1997) and Toda and Stein (2002).

The angle θ between the major discontinuity and the regional S_H stress axis is of 62° for the northwestern tip of the El Castillo de las Guardas fault (Fig. 4). The values obtained for the α and β angles from the stress field computed after the use of the Reches et al. (1992) fault slip inversion method are of 27° and 21°, respectively (Fig. 4A). Instead, when incomplete fault systems (Camacho, 1999) are taken into account, the estimated values are $\alpha = 17°$ and $\beta = 40°$ (Fig. 4B). Analysis of the stress trajectories determined from the study of diabase dykes yields $\alpha = 11°$ (Fig. 4C). It must be highlighted that, because the uncertainties in the stress trajectories due to the uneven distribution of measurement sites discussed above, the comparison between the determined stress field and theoretical models must be considered as a purely qualitative analysis. In any case, according to Homberg et al. (1997), the largest deviations in the stress trajectories (large α values) are obtained in the extensional domains for $\theta < 45°$. Instead, values of $\theta > 45°$ generate large deviations in the contractional domains (large β values), in coincidence with the deviation of the stress trajectories obtained for the El Castillo de las Guardas fault in Fig. 4B (stress determination corrected after the method of Camacho, 1999). Fig. 7 shows the comparison between the determined stress trajectories and the predictions of the model of Homberg et al. (1997). The best fit is obtained for the case with $(\sigma_1-\sigma_3) = 50$ MPa and $\mu = 0.01$. Indeed, the actual values of the α and β angles increase with the applied regional differential stress and with the amount of slip along the master fault, and decrease with the friction coefficient. These variables cannot be constrained from our results because neither the stress ellipsoid nor the friction coefficient is homogeneously distributed across the studied zone (Table 1), and the comparison shown in Fig. 7 must only be viewed as of a geometric and not dynamic nature. In any case, the deviation in stress trajectories is indicative of a sinistral strike-slip displacement of the El Castillo de las Guardas fault during the Moscovian (fault system A).

Application of the model of Toda and Stein (2002) to the studied zone has considered an average azimuth of $S_H = N55°E$, and the main parameters (stress ratio, friction coefficient and fault displacement) have been varied such to obtain the best fit with the measured faults. The best solution was found for a stress ratio, $R = (\sigma_2-\sigma_3)/(\sigma_1-\sigma_3) = 0.89$, a Poisson's ratio $\nu = 0.25$ and a depth of 4 km. The stress ratio is somewhat high, although it falls within the

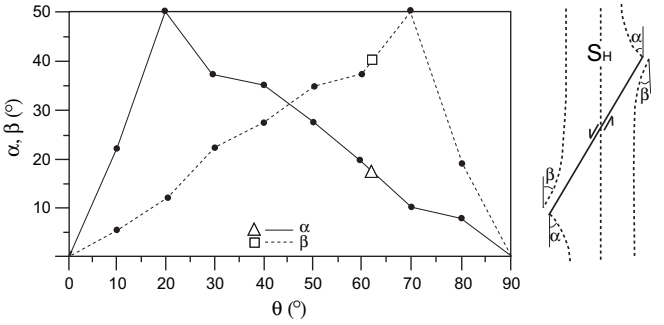

Fig. 7. Projection of angles α and β (graphically described to the right) against angle θ (explanation in the main text) according to the model of Homberg et al. (1997) for $(\sigma_1-\sigma_3) = 50$ MPa and $\mu = 0.01$. The large open triangle and square correspond, respectively, to the values of α and β determined in this work (Fig. 4B).

range of the estimated values (Table 1). The used Poisson's ratio is a very common value for average crustal rocks and rock masses (Gercek, 2006). Finally, the sub-volcanic character of most rocks in the Castilblanco de los Arroyos batholith (de la Rosa, 1992) agrees with the aforementioned depth of faulting. Spatial variation of the friction coefficient is not allowed in the method of Toda and Stein (2002). The best fit of the model with the measured faults was found for $\mu = 0.5$, which is near the mean value determined in this work (Table 1) and that is also near the constraints of the Byerlee's law for high normal stress. The results are shown in Figs. 8 and 9. The strike and kinematics of the observed small faults in the vicinity of the El Castillo de las Guardas fault acceptably match the predictions of the model (Fig. 8). The observed slip sense is in agreement with the model for strike-slip faults, although the normal faults observed at distinct locations of the El Castillo de las Guardas fault and the Cala dam fault (Fig. 9) are not predicted by the model, unless unreasonable high relative displacement along the master fault (37% of the fault length, around 17 km) are considered. The deviations of stress trajectories reproduced by the model are qualitatively similar to those observed (compare Figs. 4 and 9), albeit the model yields values of the α and β angles that are systematically lower than those determined in the natural case.

In summary, the pattern of stress trajectories obtained with the methods of Homberg et al. (1997) and Toda and Stein (2002) shows

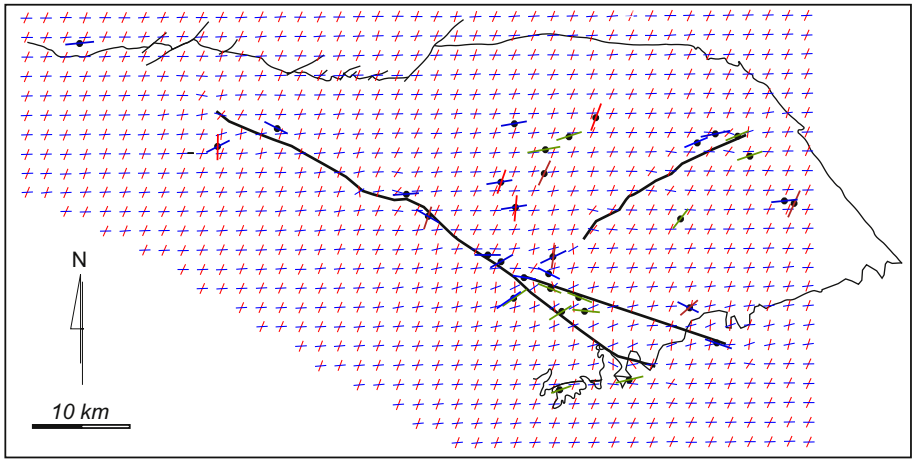

Fig. 8. Map of optimally oriented faults (small straight segments in a square grid) deduced for the studied area according the method of Toda and Stein (2002) for $\mu = 0.5$, and comparison with the average azimuth of the measured faults at distinct sites (large straight segments). Large black lines: major faults. Blue lines: small-scale sinistral faults. Red lines: small-scale dextral faults. Green lines: small-scale normal faults. (For interpretation of the references to colour in this figure legend, the reader is referred to the web version of this article.)

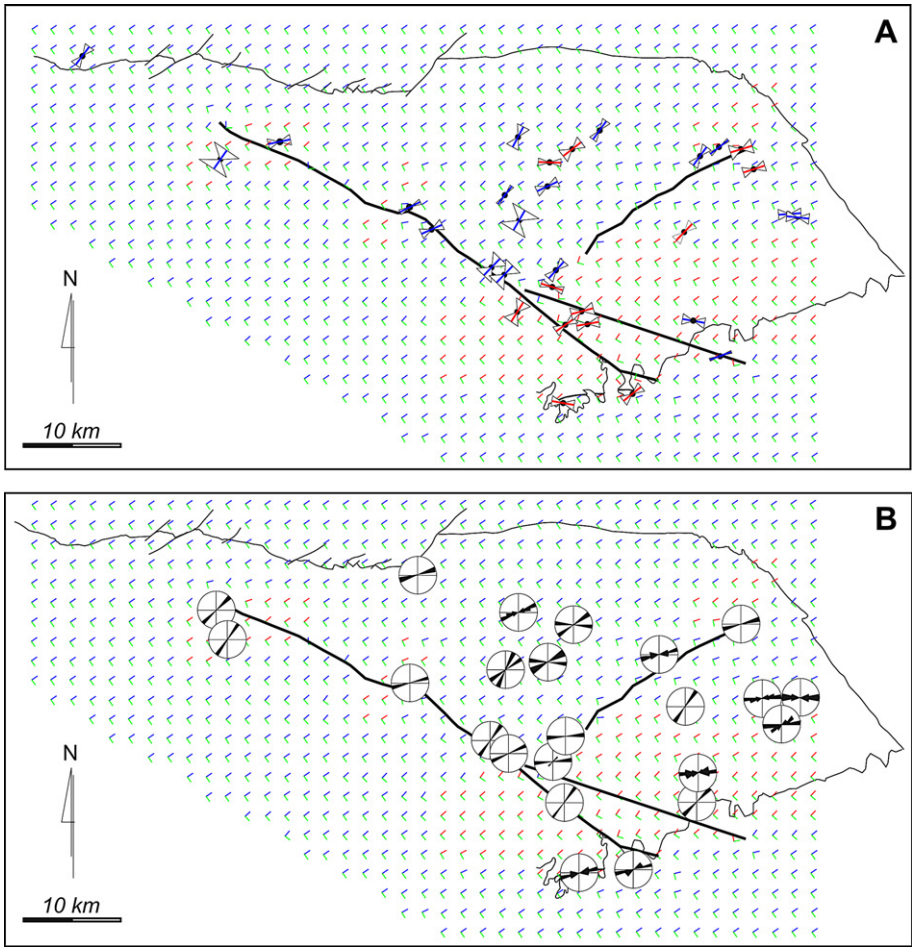

Fig. 9. Stress field predicted by the method of Toda and Stein (2002) for the studied area ($\mu = 0.5$) and comparison with A) the azimuth of the stress axes determined at each measurement site (average orientation and confidence interval calculated from the methos of Reches et al., 1992), and B) the maximum compressive axis determined from the analysis of the diabase dykes. The azimuth of the principal stress axes is marked with small straight segments in a square grid. Blue lines: σ_1. Red lines: σ_2. Green lines: σ_3.

remarkable geometrical resemblance with the Moscovian stress field determined in the studied area, although precise quantitative implications cannot been extracted from the available data. The most salient feature of the comparison between both models is again the lower values of the angles α and β yielded by the model of Toda and Stein (2002). Previous fieldwork based on the study of minor faults, stylolites or tension gashes (e.g., Petit and Mattauer, 1995) shows that deviation of stress trajectories around major faults are more in accordance with the model of Homberg et al. (1997).

Limitations of the used models to quantitatively constrain the conditions of the brittle deformation near the El Castillo de las Guardas fault are a consequence of its complex geometry, with several along-strike changes in azimuth (Fig. 1), and of the inherently heterogeneous spatial distribution of rock types and, consequently, in the values of the relevant mechanical parameters. Large slips along faults activate inelastic deformation of the rocks, particularly close to the fault termination. Given the fact that the Cala dam fault shows an accumulated displacement of around 7 km, mostly during the Moscovian, while a similar value (although not yet determined) should be assigned to the Moscovian slip of El Castillo de las Guardas fault according to its large comparative length (Fig. 1), comparison with models assuming that the crust behaves as a linear, elastic solid is by no means straightforward. Again, using of these commonly accepted models must be merely envisaged as a qualitative approximation to the real complex problem. Also the presence of oblique-slip components in the measured faults, with a complex spatial variation from predominantly strike-slip to normal fault populations cannot be easily considered in the available models and it produces some mismatches (e.g., Fig. 8) hindering the qualitative interpretation of the results. Nevertheless, there is a direct relationship between the anisotropy of the faulted crust and the deviation of regional stress trajectories (Chester and Fletcher, 1997). The case of the El Castillo de las Guardas fault shows that theoretical models can be satisfactorily used to obtain a first-order approximation to explain the geometry and kinematics of small faults generated around reactivated major structures.

5. Conclusions

The analysis of the regional stress deviation around a major, crustal-scale fault can be done by comparing the stress trajectories determined from the use of fault-slip inversion methods upon outcrop-scale fault populations, with the predictions of the available theoretical models. The case of the El Castillo de las Guardas fault, a late Palaeozoic structure that accommodated large displacements at the South Portuguese Zone of the Variscan Iberian Massif, shows that theoretical models like those of Homberg et al. (1997) or Toda and Stein (2002) cannot be used yet to gain a precise quantitative knowledge of natural palaeostress perturbations around large faults. However, both the slip sense of the master fault and the general spatial distribution, geometry and kinematics of the small faults

around it can be adequately explained by this procedure. In particular, it has been here concluded that the El Castillo de las Guardas fault suffered a sinistral strike-slip displacement during the Moscovian (Late Carboniferous), and that as a result of it a complex perturbation of the regional stress field was generated at the tips and along-strike bends of this crustal-scale fault. Future efforts in the field of theoretical modelling should consider the spatially -and temporally- variable nature of the parameters controlling the mechanical behaviour of the brittle continental crust, and the common identification of natural fault populations with predominantly oblique slip.

Acknowledgements

This study was financed by the Junta de Andalucía (PAIDI, RNM-310) and University of Huelva (Plan Propio de Investigación). The constructive reviews and comments of Ze'ev Reches and an anonymous reviewer improved substantially the manuscript and are gratefully acknowledged.

References

Ábalos, B., Díaz Cusí, J., 1995. Correlation between seismic anisotropy and major geological structures in SW Iberia: a case study on continental lithosphere deformation. Tectonics 14, 1021–1040.
Anderson, E.M., 1951. The Dynamics of Faulting and Dyke Formation with Applications to Britain. Oliver and Boyd, Edinburgh.
Angelier, J., 1994. Fault slip analysis and paleostress reconstruction. In: Hancock, P. (Ed.), Continental Deformation. Pergamon, Oxford, pp. 101–120.
Bard, J.P., 1969. Le métamorphisme régional progessif de Sierra de Aracena en Andalousie occidentale (Espagne). Ph.D. thesis, University of Montpellier, France.
Bieniawski, Z.T., 1989. Engineering Rock Mass Classifications. John Wiley & Sons, New York.
Byerlee, J.D., 1978. Friction in rocks. Pure and Applied Geophysics 116, 615–626.
Camacho, M.A., 1999. Tectónica reciente y campos de esfuerzos en el suroeste de la Península Ibérica. M.Sc. thesis, University of Huelva.
Casas-Sáinz, A., Maestro-González, A., 1996. Deflection of a compressional stress field by large scale basement fault: a case study from the Tertiary Almazán basin (Spain). Tectonophysics 255, 135–156.
Chester, J.S., Fletcher, R.C., 1997. Stress distribution and failure in anisotropic rock near a bend on a weak fault. Journal of Geophysical Research 102, 693–708.
Chinnery, M.A., 1966. Secondary faulting. Canadian Journal of Earth Sciences 3, 163–190.
Cocco, M., King, G.C.P., Nostro, C., 1999. Fault Interaction and Stress Changes: Recent Advances and New Horizons. Report for the C.E. FAUST Project. Alicante, January 1999.
Colmenero, J.R., Fernández, L.P., Moreno, C., Bahamonde, J.R., Barba, P., Heredia, N., González, F., 2002. Carboniferous. In: Gibbons, W., Moreno, T. (Eds.), The Geology of Spain. Geological Society of London, pp. 93–116.
Cowie, P.A., Scholz, C.H., 1992. Physical explanation for the displacement-length relationship of faults using a post-yield fracture mechanics model. Journal of Structural Geology 14, 1133–1148.
Crespo-Blanc, A., Orozco, M., 1988. The southern Iberian Shear Zone: a major boundary in the Hercynian folded belt. Tectonophysics 148, 221–227.
Crespo-Blanc, A., Orozco, M., 1991. The boundary between the Ossa-Morena and south Portuguese zones (southern Iberian Massif): a major suture in the European Hercynian chain. Geologische Rundschau 80, 691–702.
de la Rosa, J.D., 1992. Petrología de las rocas básicas y granitoides del Batolito de la Sierra Norte de Sevilla, Zona Sudportuguesa, Macizo Ibérico. Ph.D. thesis, University of Seville, Spain.
de Vicente, G., 1988. Análisis poblacional de fallas. El sector de enlace Sistema Central-Cordillera Ibérica. Ph.D. thesis, University Complutense of Madrid, Spain.
Díaz-Azpiroz, M., Fernández, C., 2005. Kinematic analysis of the southern Iberian shear zone and tectonic evolution of the Acebuches metabasites (SW Variscan Iberian Massif). Tectonics 24. doi:10.1029/2004TC001682.
Díaz-Azpiroz, M., Fernández, C., Castro, A., El-Biad, M., 2006. Tectonometamorphic evolution of the Aracena metamorphic belt (SW Spain) resulting from ridge-trench interaction during Variscan plate convergence. Tectonics 25. doi:10.1029/2004TC001742.
Engelder, T., 1993. Stress Regimes in the Lithosphere. Princeton University Press, Princeton, New Jersey.
García-Navarro, E., Fernández, C., 2004. Final stages of the Variscan orogeny at the Southern Iberian Massif: lateral extrusion and rotation of continental blocks. Tectonics 23. doi:10.1029/2004TC001646.
García-Navarro, E., de la Rosa, J.D., Fernández, C., Castro, A., 2003. Caracterización geoquímica y tectonomagmática de los haces de diques básicos del extremo oriental de la Zona Sudportuguesa. Geogaceta 33, 99–102.
Gercek, H., 2006. Poisson's ratio values for rocks. International Journal of Rock Mechanics and Mining Sciences 44, 1–13.
Giese, U., Glodny, J., Kramm, U., 1993. The Gil Márquez Intrusion, SW Spain: Syntectonic Intrusion, Magma-mixing and Deformation in Transpressive Regime. In: Geological Society of America Abstracts with Programs, A-342.
Hancock, P.L., 1985. Brittle microtectonics: principles and practice. Journal of Structural Geology 7, 437–457.
Homberg, C., Angelier, J., Bergerat, F., Lacombe, O., 1994. Nouvelles données tectoniques dans le Jura externe: apport des paléocontraintes. Comptes Rendus de l'Académie des Sciences, Paris 318, pp. 1371–1377.
Homberg, C., Hu, C.J., Angelier, J., Bergerat, F., Lacombe, O., 1997. Characterization of stress perturbations near major fault zones: insights from 2-D distinct-element numerical modelling and field studies (Jura mountains). Journal of Structural Geology 19, 703–718.
Homberg, C., Angelier, J., Bergerat, F., Lacombe, O., 2004. Using stress deflections to identify slip events in fault systems. Earth and Planetary Science Letters 217, 409–424.
Jaeger, J.C., Cook, N.G.W., 1979. Fundamentals of Rock Mechanics, third ed. Chapman and Hall, London.
Julivert, M., Fontbote, J.M., Ribeiro, A., Conde, L., 1974. Mapa Tectónico de la Península Ibérica y Baleares. IGME, Madrid. E: 1/1000000.
King, G.C.P., Stein, R.S., Lin, J., 1994. Static stress changes and the triggering of earthquakes. Bulletin of the Seismological Society of America 84, 935–953.
Krantz, R.W., 1988. Multiple fault sets and three-dimensional strain: theory and application. Journal of Structural Geology 10, 225–237.
Lajtai, E.Z., 1968. Brittle fracture in direct shear and the development of second order faults and tension gashes. In: Baer, A.J., Norris, D.K. (Eds.), Proceedings Conference on Research in Tectonics, Geological Survey of Canada GSC Paper 68/52, pp. 96–112.
Lee, J.C., Angelier, A., 1994. Paleostress trajectories maps based on the results of local determinations: the "lissage" program. Computers and Geosciences 20, 161–191.
Maerten, L., Gillespie, P., Pollard, D.D., 2002. Effect of local stress perturbation on secondary fault development. Journal of Structural Geology 24, 145–153.
Mandl, G., 1988. Mechanics of Tectonic Faulting. Models and Basic Concepts. Elsevier, Amsterdam.
Mantero, E., García-Navarro, E., Alonso-Chaves, F.M., Martín Parra, L.M., Matas, J., Azor, A., 2007. La Zona Sudportuguesa: propuesta para la division de un bloque continental en dominios. Geogaceta 43, 27–30.
Marrett, R.A., Allmendinger, R.W., 1990. Kinematic analysis of fault-slip data. Journal of Structural Geology 12, 973–986.
McKinstry, H.E., 1953. Shears of the second order. American Journal of Science 251, 401–414.
Nieto-Samaniego, A.F., 1999. Stress, strain and fault patterns. Journal of Structural Geology 21, 1065–1070.
Petit, J.P., Barquins, M., 1990. Fault propagation in mode II conditions: comparison between experimental and mathematical models. Applications to natural features. In: Rossmanith, H.P. (Ed.), Mechanics of Jointed and Faulted Rocks. Balkema, Rotterdam, pp. 213–220.
Petit, J.P., Mattauer, M., 1995. Paleostress superimposition deduced from mesoscale structures in limestones: the Matelles exposures, Languedoc, France. Journal of Structural Geology 17, 245–256.
Pollard, D.D., Segall, P., 1987. Theoretical displacements and stresses near fractures in rock: with applications to faults, joints, veins, dikes, and solution surfaces. In: Atkinson, B.K. (Ed.), Fracture Mechanics of Rock. Academic Press, London, pp. 277–349.
Price, N.J., 1968. A dynamic mechanism for the development of second order faults. In: Baer, A.J., Norris, D.K. (Eds.), Proceedings Conference on Research in Tectonics, Geological Survey of Canada GSC Paper 68/52, pp. 79–95.
Quesada, C., 1998. A reappraisal of the structure of the Spanish segment of the Iberian Pyrite belt. Mineralium Deposita 33, 31–44.
Reches, Z., Dieterich, J.H., 1983. Faulting of rocks in three dimensional strain fields, I. Failure of rocks in polyaxial, servo-control experiments. Tectonophysics 95, 11–132.
Reches, Z., Baer, G., Hatzor, I., 1992. Constraints on the strength of the upper crust from stress inversion of fault slip data. Journal of Geophysical Research 97, 12481–12493.
Ribeiro, A., Munhá, J., Dias, R., Mateus, A., Pereira, E., Ribeiro, L., Fonseca, P., Araújo, A., Oliveira, T., Romao, J., Chaminé, H., Coke, C., Pedro, J., 2007. Geodynamic evolution of the SW Europe Variscides. Tectonics 26. doi:10.1029/2006TC002058.
Scholz, C.H., 1990. The Mechanics of Earthquakes and Faulting. Cambridge University Press, Cambridge, UK.
Scholz, C.H., 1998. Earthquakes and friction laws. Nature 391, 37–42.
Schwartz, D.P., Sibson, R.H. (Eds.), 1989. Fault segmentation and controls of rupture initiation and termination. United States Geological Survey Open-File Report, pp. 89–315.
Sierra, S., 2003. Análisis estratigráfico de la Cuenca Pérmica del Viar (SO de España), Ph.D. thesis, University of Huelva, Spain.
Silva, J.B., Oliveira, J.T., Ribeiro, A., 1990. Structural outline. South Portuguese zone. In: Dallmeyer, R.D., Martinez Garcia, E. (Eds.), Pre-Mesozoic Geology of Iberia. Springer, Berlin, pp. 348–363.
Simancas, J.F., 1983. Geología de la extremidad oriental de la Zona Sudportuguesa, Ph.D. thesis, University of Granada, Spain.

Simancas, J.F., 1985. Una zona de cizalla frágil tardía en el límite entre Ossa Morena y la Zona Sudportuguesa (Macizo Ibérico). Cuadernos de Geología 12, 105–112. Universidad de Granada.

Simancas, J.F., Carbonell, R., González Lodeiro, F., Pérez-Estaún, A., Juhlin, C., Ayarza, P., Kashubin, A., Azor, A., Martínez Poyatos, D., Almodóvar, G.R., Pascual, E., Sáez, R., Expósito, I., 2003. The Crustal structure of the transpressional Variscan Orogen of SW Iberia: the IBERSEIS deep seismic reflection profile. Tectonics 226. doi:10.1029/2002TC001479.

Simón, J.L., Arlegui, L.E., Liesa, C.L., Maestro, A., 1999. Stress perturbations registered by jointing near strike-slip, normal, and reverse faults: examples from the Ebro Basin, Spain. Journal of Geophysical Research 104, 15141–15153.

Toda, S., Stein, R.S., 2002. Response of the San Andreas fault to the 1983 Coalinga-Nuñez Earthquakes: an application of interaction-based probabilities for Parkfield. Journal of Geophysical Research 107. doi:10.1029/2001JB000172.

Twiss, R.J., Unruh, J.R., 1998. Analysis of fault-slip inversions: do they constrain stress or strain rate? Journal of Geophysical Research 103, 12205–12222.

Zoback, M.D., Zoback, M.L., Mount, V.S., Suppe, J., Eaton, J.P., Healy, J.H., Oppenheimer, D., Reasenberg, P., Jones, L., Raileigh, C.B., Wong, I.G., Scotti, O., Wentworth, C., 1987. New evidence on the state of stress of San Andreas fault system. Science 238, 1105–1111.